

Supplementary Information for

Mirror-enhanced super-resolution microscopy

Xusan Yang^{✉,1}, Hao Xie^{✉,1,2}, Eric Alonas^{✉,2}, Yujia Liu^{1,3}, Xuanze Chen¹,
Philip J. Santangelo², Qiushi Ren¹, Peng Xi^{1,2,3,4,‡}, and Dayong Jin^{3,4}

¹Department of Biomedical Engineering, College of Engineering, Peking University, No. 5 Yiheyuan Road, Beijing 100871, China

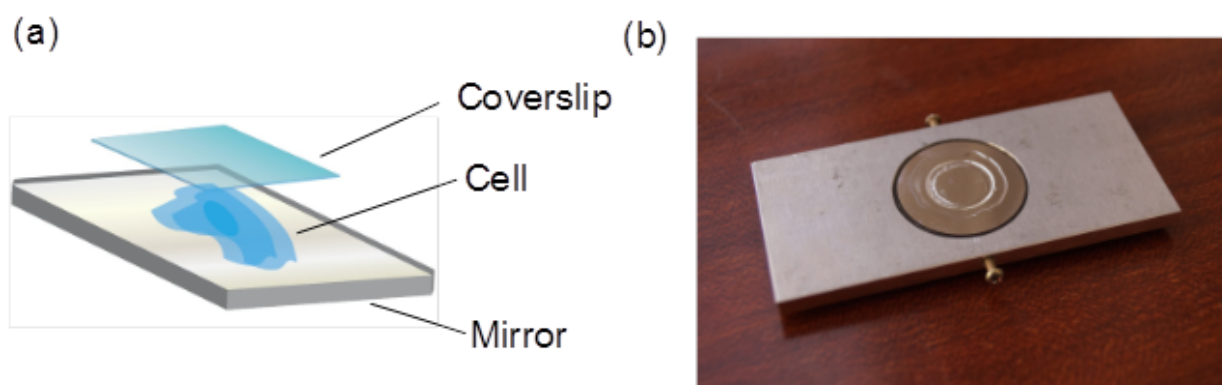
²Wallace H Coulter Department of Biomedical Engineering, Georgia Institute of Technology and Emory University, Atlanta, GA 30332, USA

³Advanced Cytometry Labs, ARC Centre of Excellence for Nanoscale BioPhotonics (CNBP), Macquarie University, Sydney, NSW, 2109, Australia

⁴Institute for Biomedical Materials and Devices (IBMD), Faculty of Science, University of Technology Sydney, Sydney, NSW, 2007, Australia

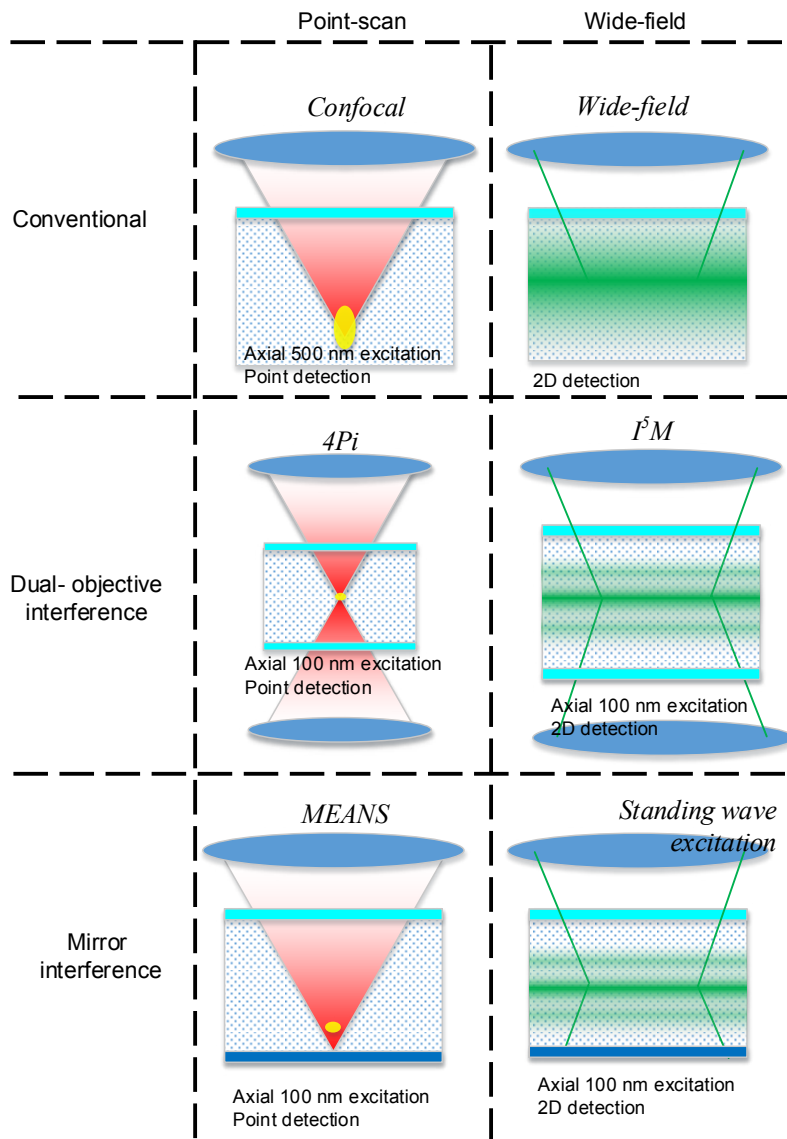
[✉]These authors contributed equally to this work.

[‡]To whom correspondence should be addressed. Email: xipeng@pku.edu.cn



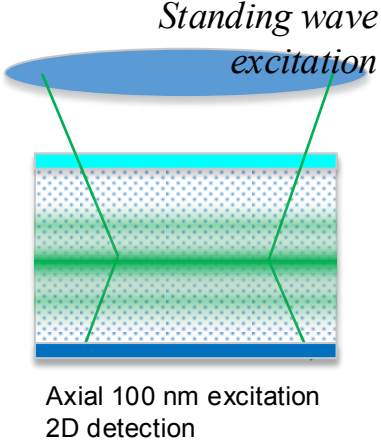
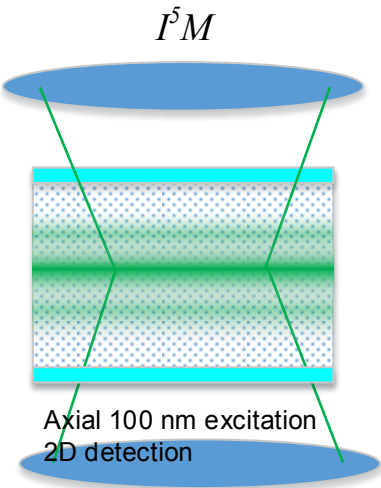
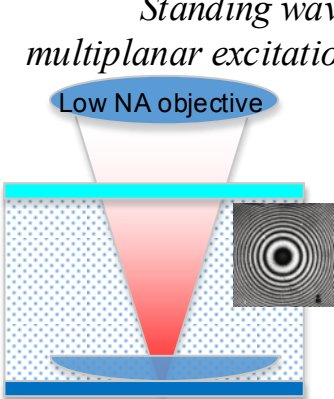
Supplementary Scheme S1 | The structure of the MEANS specimen. (a) A diagram of the specimen, in which cells are grown on top of a 50 nm silica-coated first-surface mirror (custom made). (b) A photograph of the mirror-loaded cell sample with a custom made slide adapter.

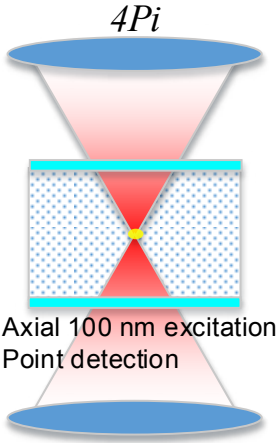
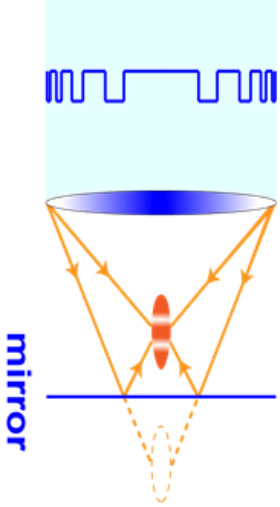
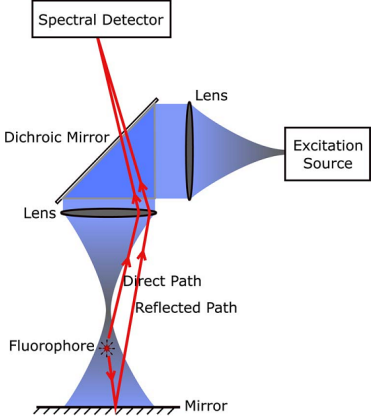
Comparison of different imaging modalities.



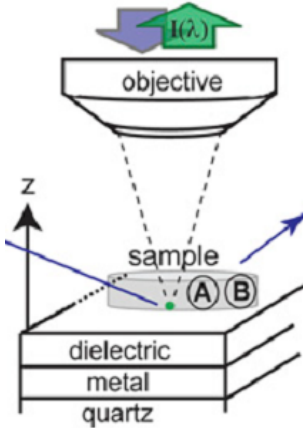
Supplementary Figure S1 | Comparison of different imaging modalities.

Supplementary Table S1 | Comparison of different interference-based techniques to improve the axial resolution.

Technique	Illustration	Description
Standing wave fluorescence microscopy (SWFM) ¹	 <p style="text-align: center;"><i>Standing wave excitation</i></p> <p style="text-align: center;">Axial 100 nm excitation 2D detection</p>	<p>Based on wide-field microscopy, it can enhance the local electromagnetic field through interference between the incidence and the reflection. However, because the out-of-focus plane fluorescence can also be excited, this technique was not demonstrated experimentally with the mirror.</p>
I^5M^2	 <p style="text-align: center;"><i>I⁵M</i></p> <p style="text-align: center;">Axial 100 nm excitation 2D detection</p>	<p>Based on wide-field microscopy of two opposing objectives, I^5M generates a thin plane of fluorescent excitation through interference. It is the first to demonstrate experimentally the wide-field axial narrowing concept.</p>
Standing wave multiplanar excitation (SWME) ³	 <p style="text-align: center;"><i>Standing wave multiplanar excitation</i></p> <p style="text-align: center;">Low NA objective</p> <p style="text-align: center;">Concentric Newton ring for axial imaging 2D detection</p>	<p>By employing a low NA objective, a flat mirror, and a plan-convex lens to load the specimen, Newton rings can be generated, in which the number of the ring denotes the axial position of the dye. It can also be used with high NA objective, in which case the mirror should be changed to a plano-convex reflector.</p>

<p>4Pi⁴</p>	 <p style="text-align: center;"><i>4Pi</i></p> <p style="text-align: center;">Axial 100 nm excitation Point detection</p>	<p>Based on confocal point-scanning microscopy with two opposing objectives, 4Pi can generate an axially narrowed PSF with 100 nm width.</p>
<p>Isotropic focusing⁵</p>	 <p style="text-align: center;">mirror</p>	<p>With phase modulation, two real focal spots are generated; one of them is then reflected by a mirror to generate 4Pi like interference.</p>
<p>Spectrally self-interference fluorescence microscopy (SSFM)⁶</p>	 <p style="text-align: center;">Spectral Detector</p> <p style="text-align: center;">Excitation Source</p> <p style="text-align: center;">Dichroic Mirror</p> <p style="text-align: center;">Lens</p> <p style="text-align: center;">Direct Path</p> <p style="text-align: center;">Reflected Path</p> <p style="text-align: center;">Fluorophore</p> <p style="text-align: center;">Mirror</p>	<p>In SSFM a mirror with spacer much larger than wavelength ($>10\lambda$) is employed. The fluorescence spectrum carrying the axial position information can be revealed through spectral detection.</p>

Spectrally coded optical nanosectioning (SpecON)⁷



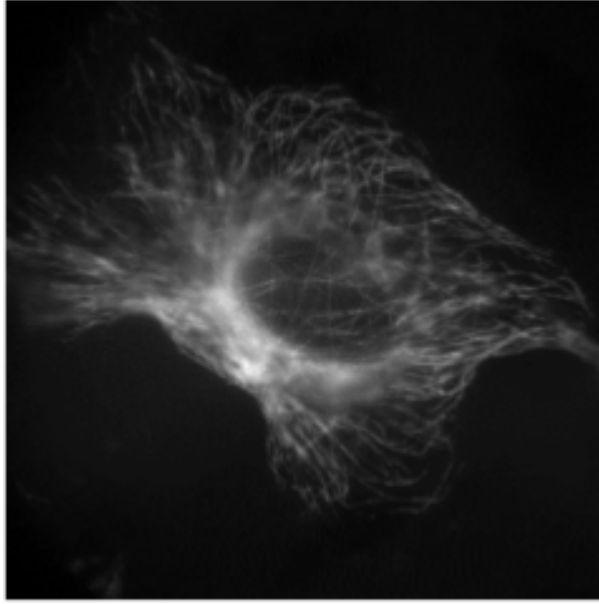
In SpecON, the sample is placed on top of a Langmuir–Blodgett thin film as spacer, before the metal layer. Through careful control of the thickness of dielectric LB film, FRET can be generated between the fluorophore and the metal, resulting in a modulation to the fluorescent emission spectrum with the axial position of the fluorophore. Nanosectioning can be obtained through the FRET analysis.

Mirror enhanced axial narrowing super-resolution (MEANS)



Axial 100 nm excitation
Point detection

In MEANS, a high NA objective is used; with the specimen loaded on a mirror, and a dielectric layer is used as spacer. The local field can be enhanced by 3.6-fold, with axially narrowing detection. The lateral resolution of STED can be improved by two-fold, with better optical sectioning capability.



Supplementary Figure S2 | The wide-field fluorescence imaging result of the same cell to supplement Figure 1 in the main text. While TIRF optically sections the superficial layer of the cell close to the coverslip and MEANS focuses the internal suspended layer of the cell above the mirror surface, wide-field microscopy images the whole depth of the cell (lacking of optical sectioning capability). Image registration has been performed to correlate the different image modalities of TIRF, MEANS and wide field using the MATLAB Image Processing Toolbox, because the MEANS image is collected with a PMT detector using a confocal laser scanning microscope and wide-field and TIRF images are collected with an EMCCD camera.

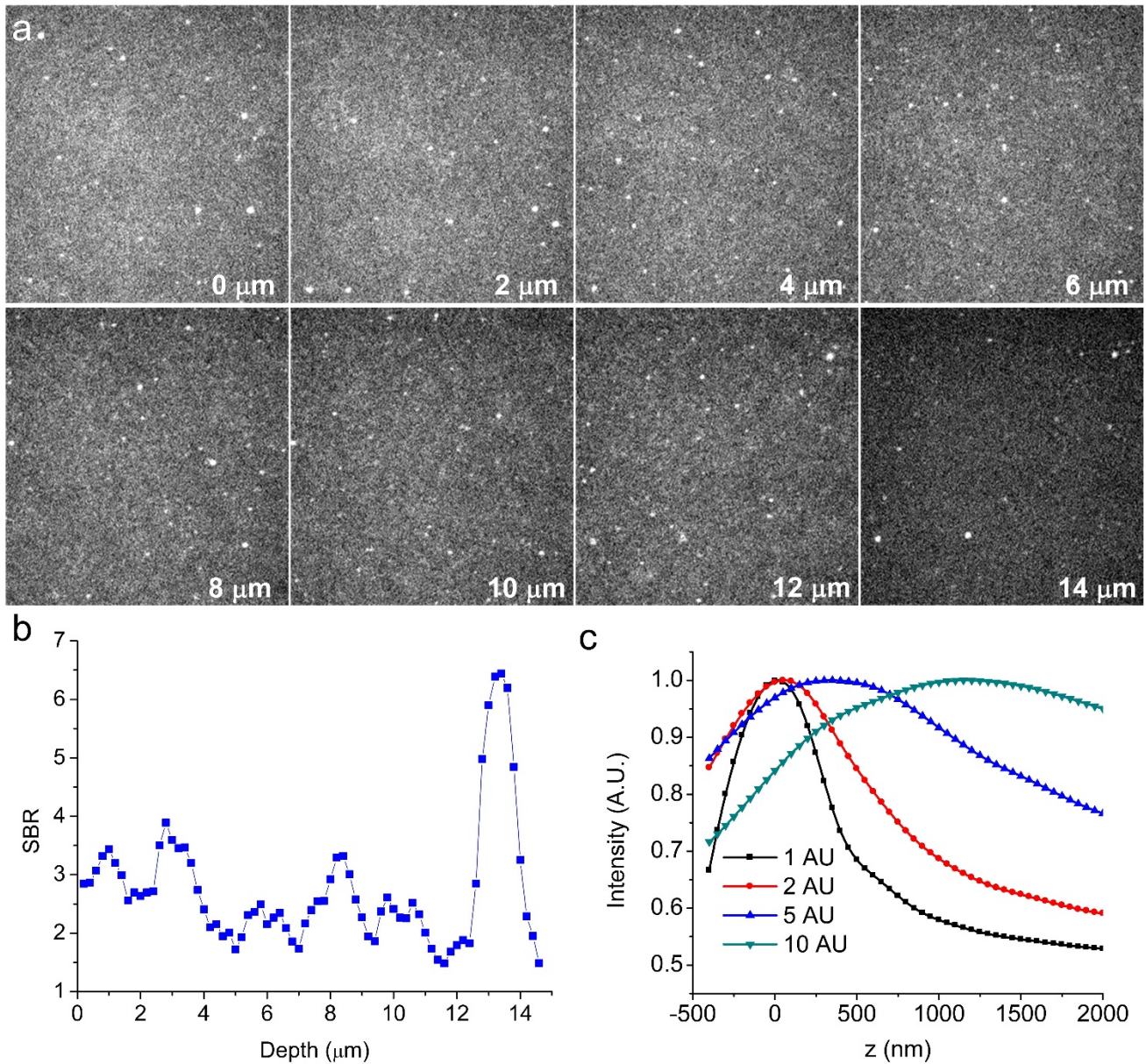
Locating the MEANS layer and determining its axial thickness

To demonstrate that the thickness of the MEANS PSF is narrower than that of confocal PSF, we used an artificial specimen with fluorescent bead scattered in agarose as our test sample, and image the MEANS/conventional confocal image. However, since the MEANS layer is fixed at a constant plane above the mirror (wavelength dependent), and it is fairly insensitive to the position of the mirror (Supplementary Videos S1) measuring the axial thickness of the PSF by optical sectioning is difficult. Instead, it is possible to measure the signal to background ratio (SBR), given the following assumptions. First, the thickness of the specimen should be inversely proportional to the SBR. Second, a decrease in the thickness of the PSF should increase the fluorescence emission intensity, assuming the fluorophore is not saturated. Third, there might also be a decrease in background, as the focal region confined. One caveat is that scattering from the incident and reflected light might also be collected, making the reduction in background less dramatic than expected.

In practice, we find that these assumptions hold true. From our images of fluorescent beads at different objective positions (Supplementary Fig. S3a), we evaluated the background noise floor by manually choosing an area with no fluorescent bead involved. We obtained a 3-fold of SBR enhancement over conventional confocal (Supplementary Fig. S3b). The axial PSF thickness of conventional confocal is ~ 735 nm (excitation wavelength $\lambda_{ex}=561$ nm, emission wavelength $\lambda_{em}=605$ nm, NA 1.3 oil-immersion, pinhole size = 1 AU).

Although the maximum photon density of MEANS is ~ 3.6 -fold that of confocal, the photon count does not scale proportionally. This is because confocal has an axially extended focal spot (~ 600 nm) than MEANS (~ 110 nm). Furthermore, the pinhole plays a role in collecting the photons more at the focal spot and less at outside, with a distribution function similar to PSF, but convolved with the size of the pinhole. This function can be termed the modulation spread function (MSF). In MEANS scenario, both excitation and detection intensity are modulated by mirror. The excitation PSF is simply the coherent superposition of incident and reflected field, while the detection MSF is also integrated over the fluorescence spectrum. Here we estimate the MSF by adding the intensity of the incoherent forward propagating and backward propagating fluorescence light, which takes into consideration of the convolution between the pinhole size and the point spread function. The net signal intensity must then be equal to the 3D integration of the MEANS PSF times the MSF. Naturally, it reduces to a normal confocal situation when the focal spot of the objective is too far away from the mirror, making the reflection contribution negligible.

The average intensity of image is calculated based on the assumption that the fluorophores are uniformly distributed in the solution. We have simulated the different situations with different pinhole size setup (Supplementary Fig. S3c). With the pinhole of 1-2 Airy Units (AU), we can see that the peak signal ($0\mu\text{m}$) is ~ 2 -fold that of confocal which is $2\mu\text{m}$ away from the mirror. Further increasing the pinhole size leads to a decrease in the enhancement, due to the increase in the confocal detection area.



Supplementary Figure S3 | The depth imaging of 20 nm fluorescent beads embedded in agarose with a mirror-loaded specimen. (a) Images of fluorescent beads at different objective depths. The mirror is located close to the 14 μm depth. The 3-fold Signal-to-background (SBR) at the 13.5 μm layer indicates a much narrower excitation field due to MEANS interference. (b) The SBR and background level plotted with respect to depth. (c) The simulated intensity distribution with respect to the axial depth for different pinhole sizes (in Airy Units). Here the mirror position is set to zero, and the z depth indicates the relative distance between the mirror and the confocal objective's focal spot.

Supplementary Video S1:

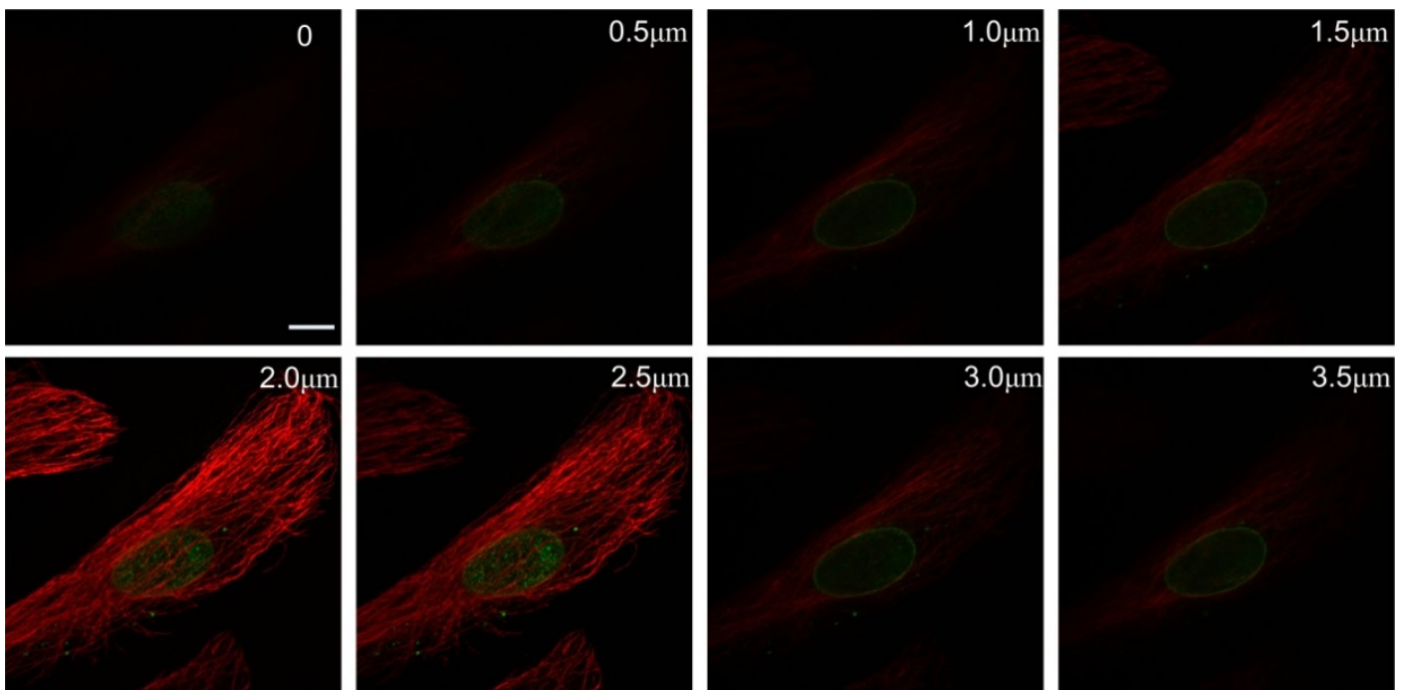
The Electromagnetic field intensity distribution for the mirror-confocal excitation is modeled, with changing the position of the mirror (denoted as the right border of the image). Objective with $n = 1.5$, N. A. = 1.4, and $\lambda_{ex}=488$ nm is used for simulation. The 0 position denotes the location of the focal spot. As can be seen, the focal enhancement can last for ~ 0.4 μm , due to the constructive interference.

Supplementary Video S2:

The electromagnetic field intensity distribution for the mirror-STED beam is modeled, with changing the position of the mirror (denoted as the right border of the image). Objective with $n = 1.5$, N. A. =1.4, and $\lambda_{de}=592$ nm is used for simulation.

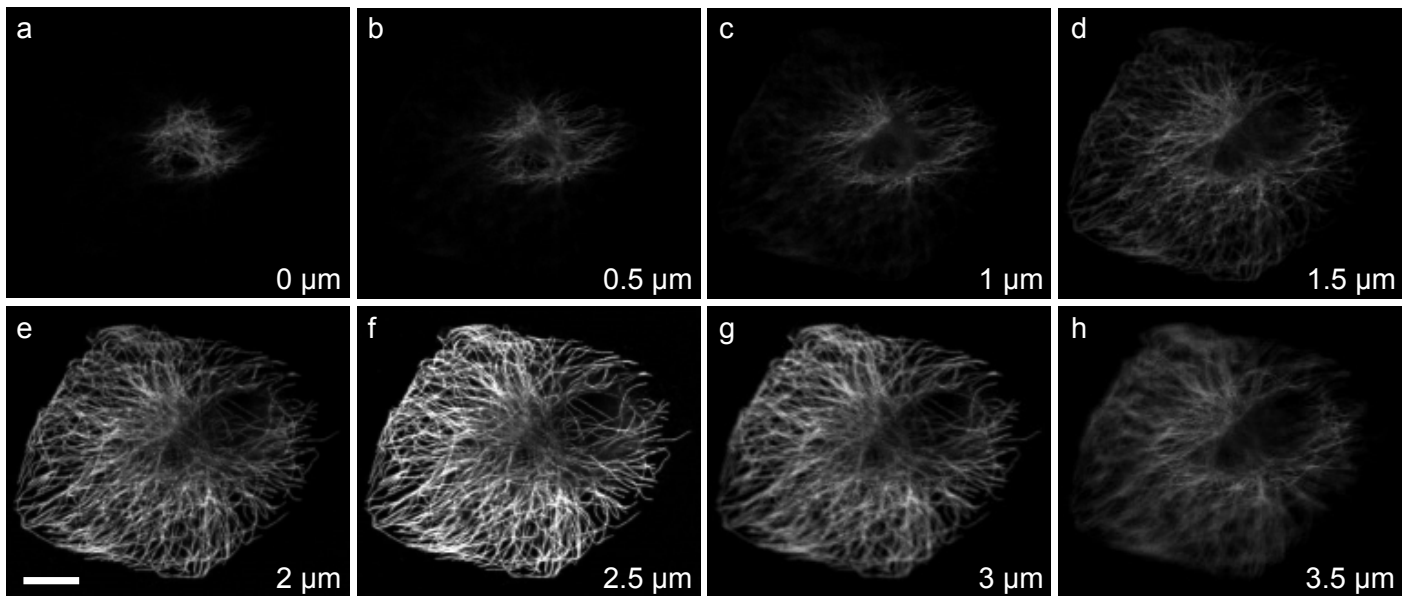
MEANS approach in spinning disk confocal microscopy

MEANS is also compatible with spinning disk confocal microscopy for high speed live cell imaging. Here we made a z-stack image of the microtubules (red) and nuclear pore complex (green) of a Vero cell grown on the mirror substrate under a commercial spinning disk microscope (UltraView VoX, PerkinElmer). We employed an oil immersion objective (100X, N. A.=1.4, Nikon), and 488 nm and 647 nm as the excitation wavelengths, respectively. Comparing the MEANS spinning disk image (2.0 μm) to the spinning disk confocal images in 0-1.5 μm , it is clear that MEANS can increase the SBR.



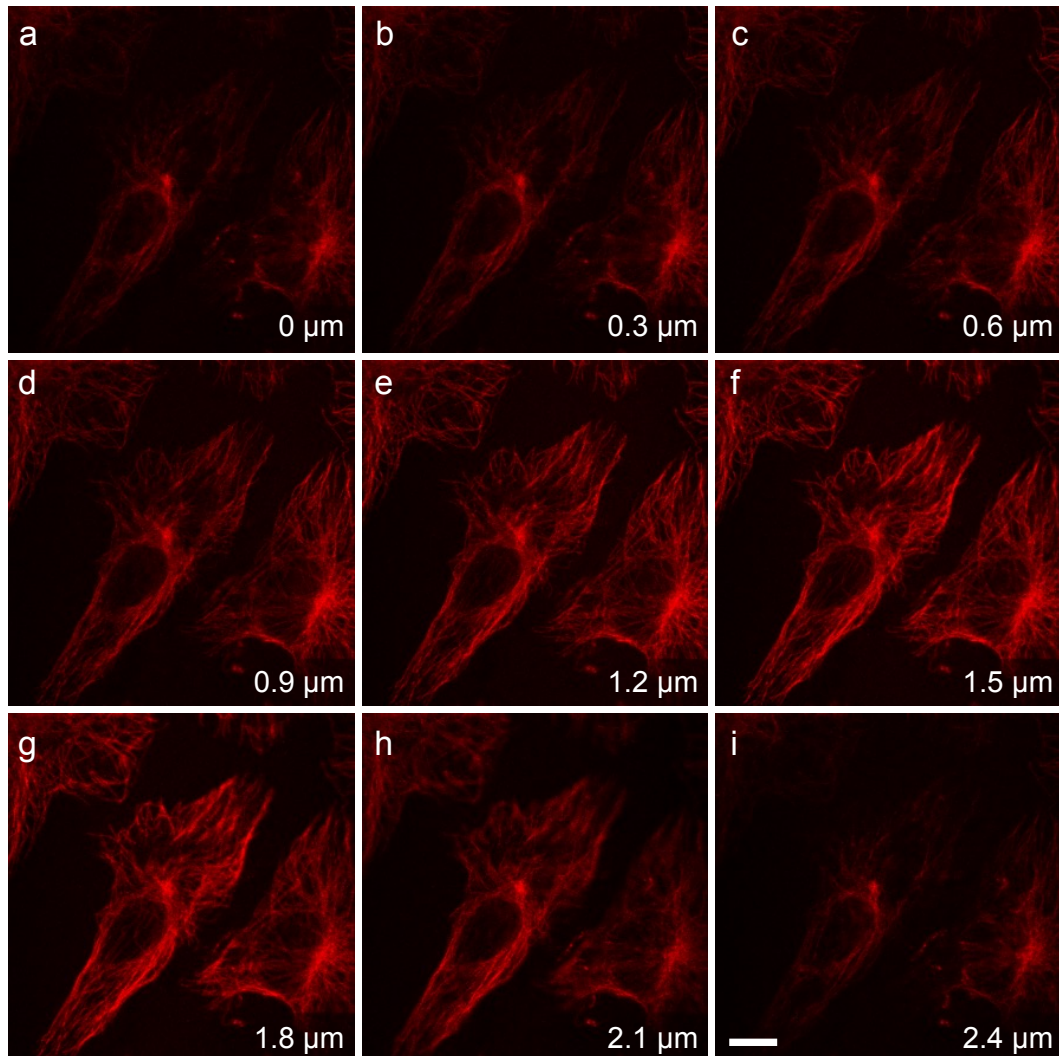
Supplementary Figure S4 | Image z-stacks of MEANS spinning disk confocal microscopy. The 8 sequential images at every 0.5 μm away from the top surface (0 μm) towards the mirror substrate were recorded. Clearly the images 0 μm – 1.5 μm were standard confocal images since those sections were still far away from the MEANS modality region. The difference between the image at 1.5 μm and the image at 2.0 μm indicated that the confocal excitation was transferred to the MEANS excitation so that a particular section of the cell suddenly showed up. The image at 2.0 μm achieved maximum SBR indicating the best interference of incident excitation beam and reflected beam. Although image at 1.5 μm and the image at 2.5 μm are at the same distance from image at 2.0 μm , the images at a distance of 3.0 μm and 3.5 μm from the top surface are heavily blurred as a result of the multiple interference maxima that arise when the focal spot is too close to the mirror. Scale bar, 10 μm .

MEANS-confocal microscopy



Supplementary Figure S5 | Image z-stacks of MEANS-confocal microscopy (Olympus FV-1200, with apochromatic 60 \times , oil-immersion objective, N.A.=1.42). The 8 sequential images at steps of every 0.5 μm away from the top surface (0 μm) towards the mirror substrate were recorded. Clearly the images (a) – (c) were the standard confocal images since those sections were still far away from the MEANS modality region. The difference between image (c) and image (d) indicated that the confocal excitation was transferred to the MEANS excitation so that a particular section of the cell suddenly appeared brighter. Four steps closer to the mirror surface recorded the same axially focused section of microtubules but with different signal to noise contrasts shown as images (d) – (h). The image (f) has achieved maximum signal to noise contrast indicating the best interference of incident excitation beam and reflected beam. Although images (d) and (h) are the same distance from image (f), the image (h) at a distance of 3.5 μm from the top surface is heavily blurred as a result from the multiple interference maxima that arise when the focal spot is too close to the mirror. When the focal spot is far away from the mirror, the axial PSF reduces to the standard confocal PSF so that the image quality of images (a)-(d) was achieved at standard confocal axial resolution. Scale bar, 10 μm .

MEANS-multiphoton microscopy



Supplementary Figure S6 | Image z-stacks of MEANS-two-photon microscopy (Zeiss LSM 710 NLO & DuoScan System, with apochromatic 63 \times , oil-immersion objective, N. A.=1.4). The 9 sequential images at steps every 0.3 μm away from the top surface (0 μm) towards the mirror substrate were recorded. The images (a) – (c) should be the standard two-photon excitation (TPE) fluorescent images, as those sections were still far away from the MEANS-TPE modality region. The difference between image (c) and image (d-f) indicated that the two-photon excitation was transferred to the MEANS excitation so that a particular section of the cell suddenly appeared brighter. The image (e-f) has achieved maximum SBR, indicating the best interference of incident excitation beam and reflected beam. Although image (d) and (h) are at the same distance from image (f), the image (h) at a distance of 2.1 μm from the top surface is more blurred (upper-left corner). Compared to the transition from confocal to confocal-MEANS, the transition from TPE to MEANS-TPE occurs faster. Vero cell microtubule stained with Dylight 650 is imaged. Scale bar, 10 μm .

MEANS-STED microscopy

Our MEANS concept can be further extended to improve the lateral resolution of conventional STED nanoscopy system, in which both the intensities of the excitation beam and the donut-shaped depletion beam can be enhanced within the MEANS region, as shown in Figure 2 in the main text. We have analyzed the interference light field of MEANS excitation and MEANS-STED. The diffraction field at coordination (r_2, ψ, z_2) can be written as⁸⁻¹⁰

$$U(r_2, \psi, z_2) = -\frac{i}{\lambda} \iint P(\theta, \phi) \exp[ikr_2 \sin \theta \cos(\phi - \psi) + ikz_2 \cos \theta] \sin \theta d\theta d\phi. \quad (1)$$

The limits of the integration in this equation are from 0 to α and 0 to 2π with respect to θ and ϕ , respectively, and $NA = n \sin \alpha$. Applying paraxial approximation to it, and substituting the apodization function $P_1(\theta, \phi) = \eta(\theta/a)$ for excitation and $P_2(\theta, \phi) = \eta(\theta/a) \exp(-i\phi)$ for depletion, where $\eta = 1$ when $|x| < 1$ and $\eta = 0$ otherwise, we can get

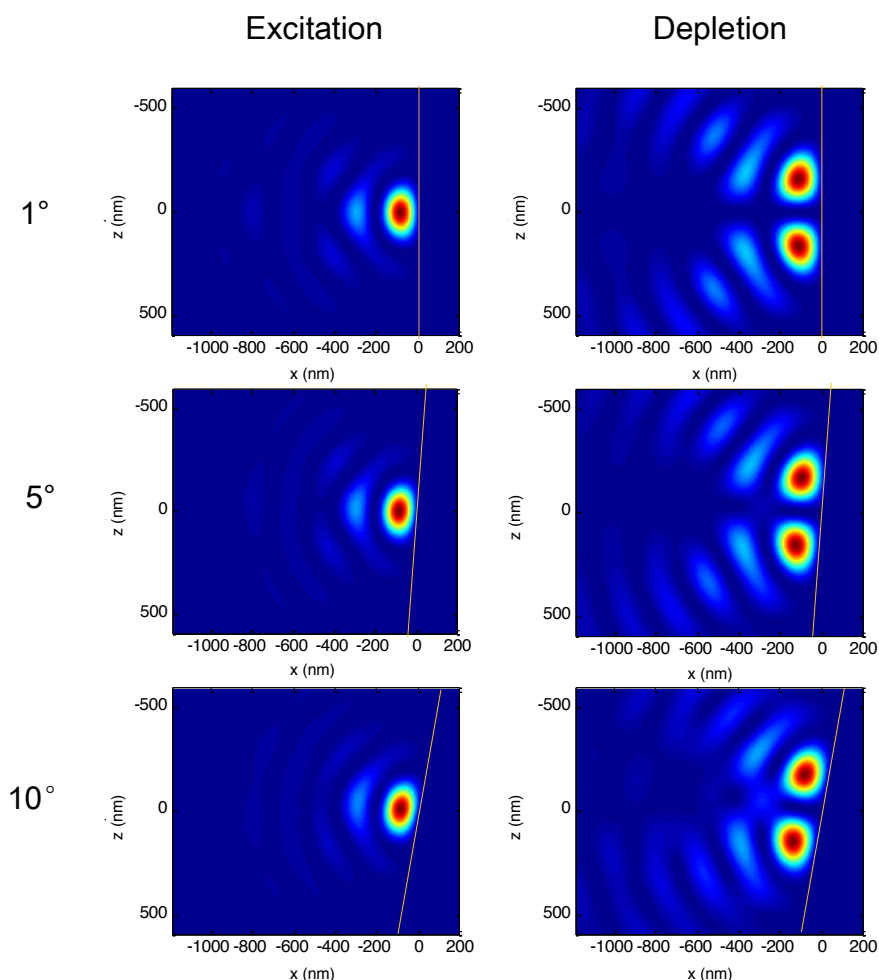
$$\begin{aligned} U_{ex}(v, u) &= A_0 \exp(ikz_2) \int_0^1 \exp\left\{-\frac{iu\rho^2}{2}\right\} J_0(\rho v) \rho d\rho, \\ U_{de}(v, u) &= A_1 \exp(ikz_2) \int_0^1 \exp\left\{-\frac{iu\rho^2}{2}\right\} J_1(\rho v) \rho d\rho \end{aligned}, \quad (2)$$

where A_0 and A_1 are two constants proportional to excitation and depletion field amplitude, $v = kr_2 \sin \alpha$, $u = 4kz_2 \sin^2(\alpha/2)$, J_0 and J_1 are the 0th and 1st order Bessel functions, respectively. The procedure of calculating the reflection field is similar to calculating the incident field, but an additional phase shift factor needs to be multiplied. This factor could be derived according to the Snell's Law. Finally, we add the complex contribution of incident and reflected field together to get the excitation and depletion field.

Experimentally, the optical quality of both the SiO₂ layer and the metal reflection layer (flatness, scratch, etc.), as well as the scattering, phase modulation, and transparency of the specimen, may affect the result.

MEANS in laser scanning confocal and STED microscopy.

In our simulation of the PSF of MEANS and MEANS-STED, the mirror is perpendicular to the incident beam. However, there may exist a small angle between optical axis of incident light and principal optical axis. We performed the PSF simulation of excitation and depletion beams when the angle is set to 1° , 5° and 10° . From Supplementary Figure S7 we can see that, such a small angle will not affect the MEANS PSF significantly. This implies that once again, the requirement of precise alignment is not as crucial as that of 4Pi. It also suggests that MEANS-STED system is also suitable for off-axis laser scanning system (galvanometric or resonant mirror scanning) for small angle ($<10^\circ$) scanning. This has also been validated in our experiments, in which different kinds of laser scanning confocal, multiphoton, and STED systems are employed.



Supplementary Figure S7 | MEANS excitation and MEANS-STED depletion PSF simulations for off-axis situation. The simulation of the excitation and depletion beams was done for 1, 5, and 10° tilt angles and for both the excitation and depletion beams.

Comparison to 3D-STED optical nanoscopy

We have also performed 3D-STED on a NPC specimen with the same staining protocol as applied in Figure 4. The same 60 mW depletion power has been applied, with 70% to improve lateral resolution and 30% to improve axial resolution. We have measured the width of the stained Nups and found that the lateral resolution is ~50 nm, due to the low depletion power (the local field for STED is 3.6-fold weaker than MEANS-STED). No Nup ring can be resolved in 3D-STED at this power. We have also performed 2D STED with 60 mW intensity, yet the Nup ring structure cannot be differentiated as well. We have also tried further increasing the depletion power in both 2D and 3D-STED, but it results in a fast photobleaching to the specimen, and the SBR of the image decreases dramatically. Because the total power that the fluorescent dye and the biological specimen is limited, MEANS-STED is favorable to biological fluorescent STED imaging, as it can provide better resolution and improved optical sectioning, without increasing the laser power.

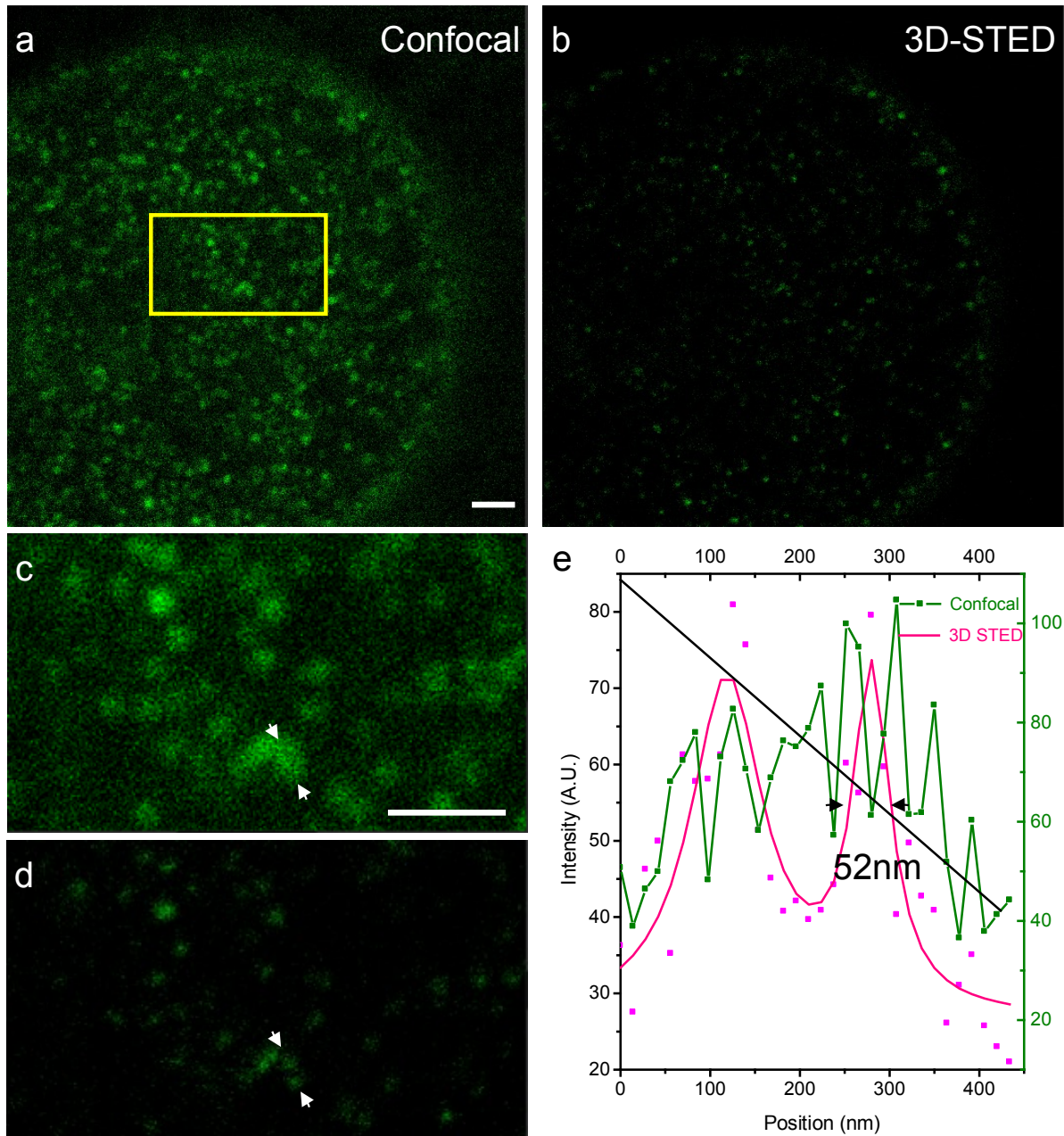
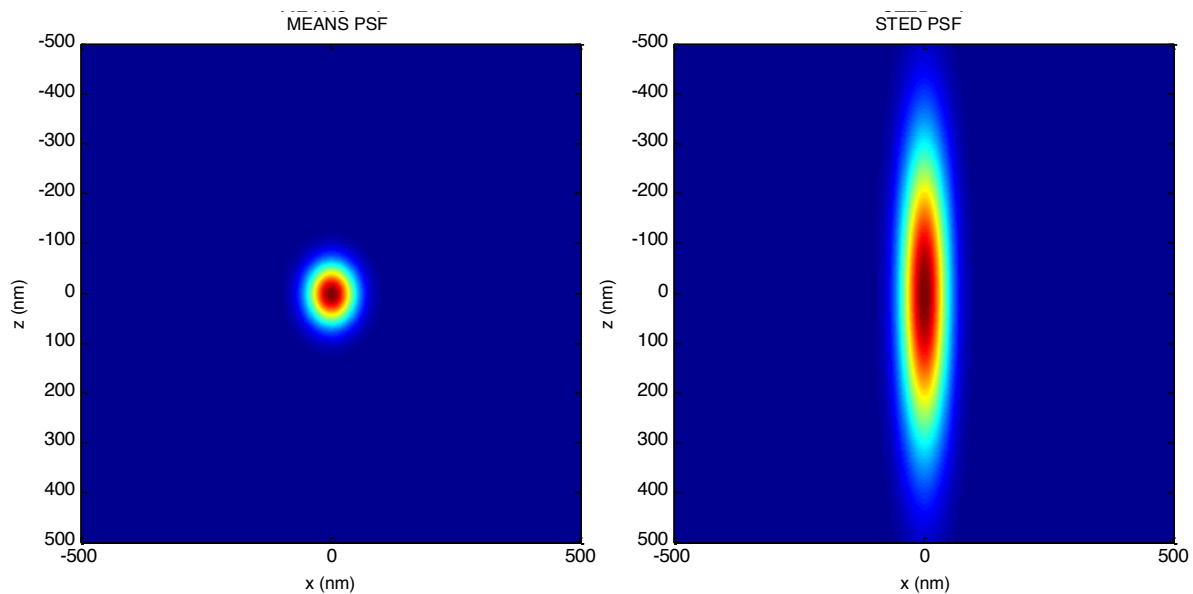


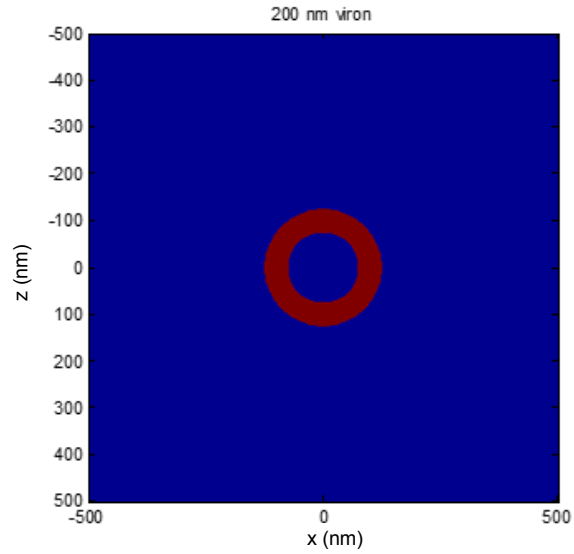
Figure S8 | 3D-STED imaging of NPC in comparison of MEANS-STED. (a) Confocal. (b) 3D-STED. (c) and (d) are zoom-in of the boxed area in (a) and (b), respectively. The intensity between the arrows is plotted in (e). The same depletion power of 60 mW is used, with 70% intensity to improve the lateral resolution and 30% for axial resolution enhancement. The lateral resolution measured by the width of the NPCs is ~ 50 nm. No Nup ring is visible in 3D-STED. Scale bar, 1 μ m.

Simulation of the importance of axial resolution enhancement in resolving the hollow structure of the viral filaments

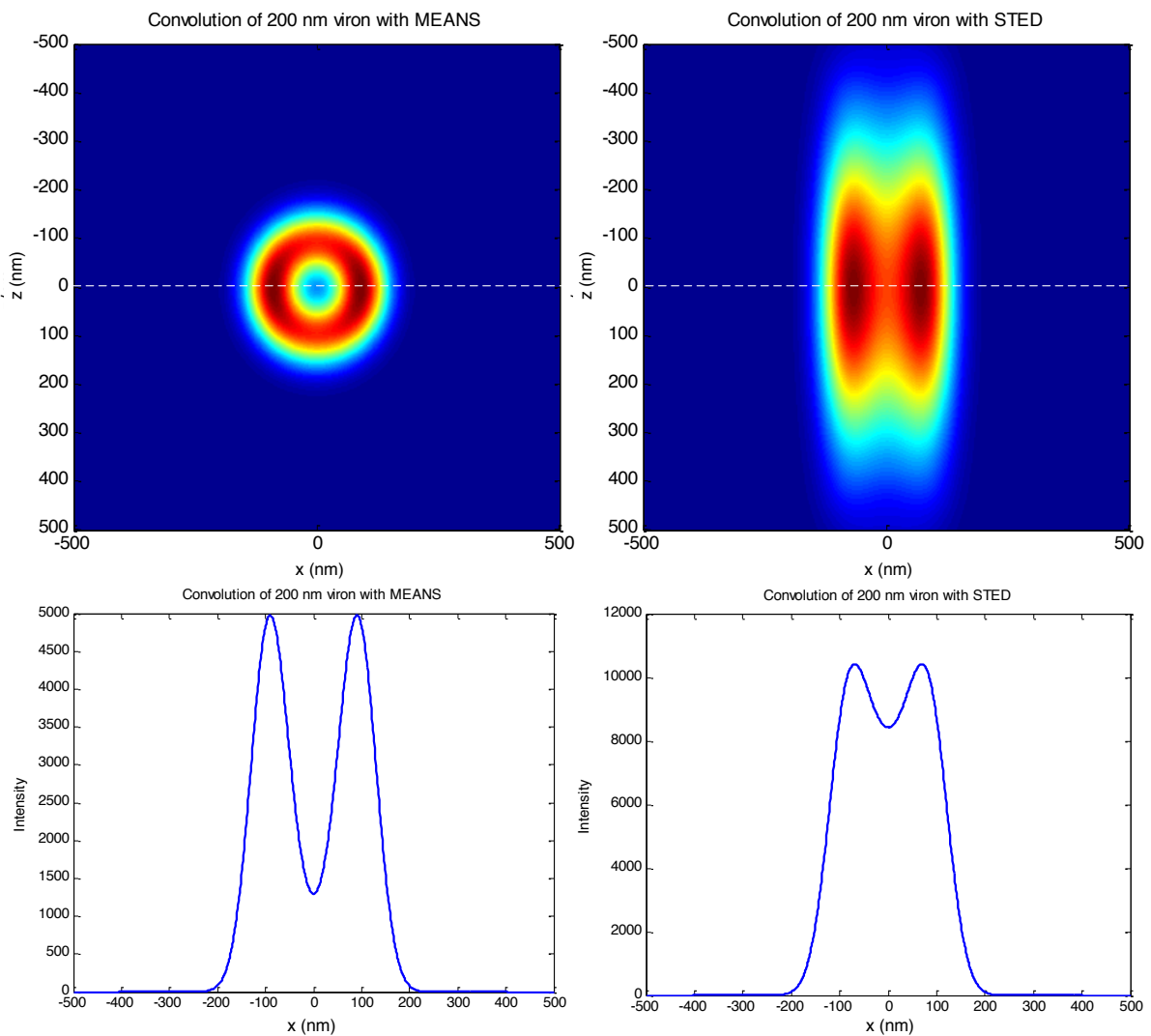
The human respiratory syncytial virus (hRSV) filament is much like a hollow cylinder lying on its side. The viral F protein coats the entire surface of the viral envelope and the viral N protein is found inside the envelope. If the axial thickness of the excitation PSF is greater than or equal to the diameter of the viral filament, the upper and lower surfaces of the viral envelope will be excited, and will decrease the contrast and the ability to resolve the sides of the viral envelope as being separated by a hollow center. To understand how the size of the PSF may affect the visualization of the hollow viral filaments, a filament with diameter of 200 nm were simulated. To demonstrate that the role of axial resolution, in the simulation, we assumed the same lateral resolution of 40 nm for both conventional STED and MEANS-STED, and different axial resolutions of 500 nm and 100 nm for STED and MEANS-STED, respectively. Images of the axial cross sections of the STED and MEANS-STED PSFs used for the simulation are shown below:



The structure of the 200 nm viral filament, with membrane thickness of 50 nm was simulated with both conventional STED and MEANS-STED. An axial cross section of the filament is shown in below:



The resulting convolution of the STED and MEANS-STED PSFs with the hollow filament is shown in Supplementary Figure S9.



Supplementary Figure S9 | Simulations to highlight the importance of axial resolution enhancement in resolving the hollow structure of viral filaments. As the viral filament F protein on the viral envelope is a tube-like hollow structure, the upper and lower surfaces of the tube can decrease the contrast using the conventional STED with axial resolution more than 500 nm. To understand how the size of axial PSF may affect the visualization of hollow viral filaments, a filament with diameter of 200 nm with membrane thickness of 50 nm is simulated. In our simulations, we assume the same lateral resolution of 40 nm can be achieved by both conventional STED and MEANS-STED, but different axial resolutions of 500 nm and 100 nm for STED and MEANS-STED, respectively. As the collected fluorescence signal is a convolution of the structure of the filament with the corresponding PSF, the conventional STED fails in providing sufficient contrast to suppress the upper and lower membranes of the 200 nm hollow structure but the MEANS modality at same lateral resolution of 40 nm can clearly resolve the hollow structure.

Supporting References

- 1 Bailey, B., Farkas, D. L., Taylor, D. L. & Lanni, F. Enhancement of axial resolution in fluorescence microscopy by standing-wave excitation. *Nature* **366**, 44-48 (1993).
- 2 Gustafsson, M., Agard, D. & Sedat, J. I5M: 3D widefield light microscopy with better than 100nm axial resolution. *Journal of Microscopy* **195**, 10-16 (1999).
- 3 Amor, R., Mahajan, S., Amos, W. B. & McConnell, G. Standing-wave-excited multiplanar fluorescence in a laser scanning microscope reveals 3D information on red blood cells. *Scientific reports* **4**, 7359 (2014).
- 4 Hell, S. W., Lindek, S., Cremer, C. & Stelzer, E. H. Measurement of the 4Pi-confocal point spread function proves 75 nm axial resolution. *Applied Physics Letters* **64**, 1335-1337 (1994).
- 5 Mudry, E., Le Moal, E., Ferrand, P., Chaumet, P. C. & Sentenac, A. Isotropic diffraction-limited focusing using a single objective lens. *Physical Review Letters* **105**, 203903 (2010).
- 6 Swan, A. K. *et al.* Toward nanometer-scale resolution in fluorescence microscopy using spectral self-interference. *Selected Topics in Quantum Electronics, IEEE Journal of* **9**, 294-300 (2003).
- 7 Elsayad, K. *et al.* Spectrally coded optical nanosectioning (SpecON) with biocompatible metal–dielectric-coated substrates. *Proceedings of the National Academy of Sciences* **110**, 20069-20074 (2013).
- 8 Wilson, T. & Sheppard, C. Theory and practice of scanning optical microscopy. *London: Academic Press*, (1984).
- 9 Watanabe, T. *et al.* Formation of a doughnut laser beam for super-resolving microscopy using a phase spatial light modulator. *Optical Engineering* **43**, 1136-1143 (2004).
- 10 Gu, M. *Advanced optical imaging theory*. Vol. 75 (Springer Science & Business Media, 2000).